Multiple circulating alkaloids and saponins from intravenous Kang-Ai injection inhibit human cytochromes P450 and UDP-glucuronosyltransferase isozymes: potential drug-drug interactions

Zifei Qin (qzf1989@163.com)
https://orcid.org/0000-0001-8989-1986
Mengmeng Jia
Zhengzhou University First Affiliated Hospital
Jing Yang
Zhengzhou University First Affiliated Hospital
Hang Xing
Zhengzhou University First Affiliated Hospital
Zhao Yin
Zhengzhou University First Affiliated Hospital
Zhihong Yao
Jinan University College of Pharmacy
Xiaojian Zhang
Zhengzhou University First Affiliated Hospital
Xinsheng Yao
Jinan University College of Pharmacy

Research

Keywords: Kang-Ai injection, pharmacokinetics, excretion, plasma protein binding rate, human cytochrome P450 (CYP), UDP-glucuronosyltransferase (UGT), drug-drug interactions (DDI)

Posted Date: May 11th, 2020

DOI: https://doi.org/10.21203/rs.3.rs-27001/v1

Version of Record: A version of this preprint was published on July 6th, 2020. See the published version at https://doi.org/10.1186/s13020-020-00349-3.

Abstract

Background

Kang-Ai injection is widely used as an adjuvant therapy drug for many cancers, leukopenia and chronic hepatitis B. Circulating alkaloids and saponins are believed to be responsible for therapeutic effects. However, their pharmacokinetics and excretion *in vivo* and the risk of drug-drug interactions (DDI) through inhibiting human cytochrome P450 (CYP) and UDP-glucuronosyltransferase (UGT) enzymes remain unclear.

Methods

Pharmacokinetics and excretion of circulating compounds were investigated in rats using a validated ultra high-performance liquid chromatography tandem mass spectrometry (UHPLC-MS) method. Further, the inhibitory effects of nine major compounds against eleven CYP and UGT isozymes were assayed using well-accepted specific substrate for each enzyme.

Results

After dosing, 9 alkaloids were found with C_{max} and $t_{1/2}$ values of 0.17–422.70 μmol/L and 1.78–4.33 h, respectively. Additionally, 28 saponins exhibited considerable systemic exposure with $t_{1/2}$ values of 0.63–7.22 h, whereas other trace saponins could be negligible or undetected. Besides, over 90% of alkaloids were excreted through hepatobiliary and renal excretion. Likewise, astragalosides and *PPT-type* ginsenosides also involved in hepatobiliary and/or renal excretion. *PPD-type* ginsenosides were mainly excreted to urine. Furthermore, *PPD-type* ginsenosides were extensively bound ($f_{u-plasma}$ approximately 1%), whereas astragalosides and *PPT-type* ginsenosides displayed $f_{u-plasma}$ values of 12.35% and 60.23–87.36%, respectively. Moreover, matrine and oxymatrine both exhibited weak inhibition against CYP3A4 with IC_{50} values of 387.40 and 604.60 μM. Similar results were observed for astragaloside IV towards CYP2C9, ginsenoside Rg1 against UGT1A1, ginsenoside Re against CYP2C8, ginsenoside Rd against CYP2B6and CYP3A4, and ginsenoside Rc against UGT1A9 with IC_{50} values between 20.19 and 92.21 μM. Ginsenoside Rb1 showed moderate inhibitory effect against CYP2C9 (IC_{50} = 8.81 μM). Through kinetic modeling, their inhibition mechanisms towards those CYP and UGT isozymes were explored with obtained K_i values. *In vitro-in vivo* extrapolation ($[I]/K_i$ = 1.15 for oxymatrine) showed the inhibition of systemic clearance for CYP3A4 substrates seemed more possible, while other major circulating compounds displayed negligible DDI risk due to $[I]/K_i$ no more than 0.1.

Conclusions

These facts lead to better understanding of chemical basis responsible for therapeutic action of Kang-Ai injection, and facilitate to pay more attention on the DDI for informing its rational clinical use.

Background

Herbal medicines are gaining popularity for the treatment of chronic and complex diseases as it works by hitting multiple molecular targets to modulate different signaling pathways [1–3]. Major advances have been made regarding their activities related their clinical indications, and more importantly in understanding their pharmacokinetics (PK) and excretion [3]. The PK profiles, just like the pharmacological activities, can be used as a “sieve” to assess the effectiveness of the individual compounds, and identify the chemical basis in an herbal injection [3–5]. Therefore, PK

behaviors and excretion of circulating compounds should be first implemented in laboratory animals to reveal their systemic exposure. The corresponding PK parameters could show the ability of herbal compounds to be absorbed and transferred from the site of administration to the action targets through multiple biological barriers, and metabolic stability *in vivo*.

Kang-Ai injection is an herbal medicine approved in 2002 by the China Food and Drug Administration (China FDA). It consists of Astragali Radix (Huangqi), Ginseng Radix et Rhizoma (Renshen) and kushenin (Kushensu), and is indicated for many cancers, leukopenia and chronic hepatitis B [6–8]. Previously, we have finished the chemical identification and content determination of the main alkaloids (oxymatrine, matrine), astragalosides (astragaloside IV) and ginseng saponins (ginsenoside Rg1, Re) in Kang-Ai injection [9]. Despite the increasing understanding of Kang-Ai injection in chemical and pharmacological studies, the systemic exposure and excretion of its bioactive compounds after administration remain to be elucidated.

Previous PK researches of individual herb or its characteristic compounds have been carried out, which greatly facilitated the holistic PK properties of Kang-Ai injection. Oxymatrine, the most abundant herbal compound in Kang-Ai injection, occupies over 95.37% of total contents. When intravenously treated with oxymatrine at 30 mg/kg, the $AUC_{0-12\ h}$, C_{max}, $t_{1/2}$ and CL values in rat plasma were 16234.27 ng·h/mL, 32847.57 ng/mL, 0.57 h and 3.10 L/h, respectively [10]. Besides, only about 19.9% of oxymatrine was reduced to matrine following intravenous infusion of 600 mg oxymatrine in healthy male volunteers [11]. In addition, systemic exposure of astragaloside IV appeared to be dose proportional over the dose ranged from 200 to 500 mL astragaloside IV (9 mg/100 mL) in healthy volunteers [12]. Furthermore, metabolism of astragaloside IV by intestinal microbiome was a crucial step in its excretion, rather than by hepatic and intestinal enzymes [13–15]. Moreover, ginsenoside Rg1, Re and Rf were not extensively bound in plasma, and also were with substantially shorter $t_{1/2}$ values and significantly larger systemic clearance ($CL_{tot,p}$) than other-type ginsenosides [16]. Although several bioanalytical assays have been applied to the PK study of several circulating alkaloids and saponins, PK and excretion information about Kang-Ai injection is still limited. This also brings a huge obstacle in our understanding of the chemical basis responsible for the therapeutic effects of Kang-Ai injection.

In addition, drug-drug interaction (DDI) is significant safety concerns in clinical medication [17–19]. Inhibition or activation of human CYP or UGT isozymes could potentially adverse clinical DDI and result in metabolic disorders for endogenous components [20–22]. It would be more serious for the clinical drugs with narrow therapeutic indices, such as digoxin, warfarin, SN-38 and so on [17]. Similarly, UGT1A1 is the only one UGT isozyme in the conjugative detoxification of bilirubin [21]. Once UGT1A1 function is inhibited, there is a high risk of liver injury [21]. Considering the intravenous administration of Kang-Ai injection and abundant exposure of its circulating herbal compounds, it should be of particularly clinical significance to investigate the potential risks of DDI.

To this goal, this current report first identified the major circulating alkaloids, astragalosides, ginsenosides in rat samples after an intravenous 30 min-infusion of Kang-Ai injection at 6 mL/kg. In addition, the detailed PK behaviors and exposure of these herbal substances in plasma were systemically carried out. Meanwhile, we also investigated the plasma binding rate assays of these circulating alkaloids and saponins. Furthermore, the excretion of these compounds in urine and bile were determined by dividing the cumulative amount excreted into urine ($Cum.A_{e-U}$) and bile ($Cum.A_{e-B}$) by their respect doses. Moreover, we explored the inhibitory effects and mechanism of nine major circulation compounds against several important CYP and UGT enzymes based on their widely recognized probe substrates. Taken together, the current PK and excretion information would facilitate the identification of active herbal compounds responsible for the therapeutic actions of Kang-Ai injection, and would also be helpful to inform its potential DDI in rational clinical use and achieve the optimal herbal therapy.

Materials And Methods

Chemicals and reagents

Kang-Ai injection samples (lot numbers of 03180805, 03181004, 01180908, 01180909, 02190102, 02190103) were manufactured by Changbaishan Pharmaceutical Co., Ltd. (Jilin, China) with China FDA drug ratification number of GuoYaoZhunZiZ-20026868. Purified matrine, oxymatrine, oxysophocarpine, isoastragaloside IV, and astragaloside III, IV, V, VI were all purchased Guangzhou Fans Biotechnology Co., Ltd (Guangzhou, China). Reference standards of ginsenoside Rb1, Rb2, Rc, Rd, Re, Rf, Rg1, Rg2, Rg6, Rh1, Rh4, Rk3, F1, F2, F3, F4, and notoginsenoside R1, R2 were all obtained from Shanghai Yuanye Biotechnology Co., Ltd. (Shanghai, China). The purity of these compounds was over 98.0%.

Magnesium chloride ($MgCl_2$), D-saccharic-1, 4-lactone monohydrate, alamethicin, nicotinamide adenine dinucleotide phosphate (NADPH), uridine 5'-diphospho-glucuronosyltransferase (UDPGA) were all obtained from Sigma-Aldrich (St. Louis, MO, USA). 4-hydroxytolbutamide, 4-hydroxymephenytoin, 4-methylumbelliferone, 6α-hydroxy-paclitaxel, 6-hydroxychlorzoxazone, 7-hydroxycoumarin, β-estradiol, bupropion, coumarin, chlorzoxazone, hydroxybupropion, mephenytoin, nifedipine, oxidized nifedipine, phenacetin, paracetamol, paclitaxel, propofol and tolbutamide were all acquired from Aladdin Chemicals (Shanghai, China). 4-MU-glucuronide, β-estradiol-3-*O*-glucuronide and propofol-*O*-glucuronide were all obtained from Toronto Research Chemicals (North York, ON, Canada). Recombinant CYP enzymes (CYP1A2, 2A6, 2B6, 2C8, 2C9, 2C19, 2E1, 3A4) and UGT isozymes (UGT1A1, 1A9, 2B7) were all provided from Corning Biosciences (Corning, NY, USA).

LC-MS-grade water, methanol and acetonitrile were purchased from Fisher Scientific (Fair Lawn, New Jersey, USA). LC-MS grade formic acid was obtained from Sigma-Aldrich (St. Louis, USA). Other reagents were of analytical or higher grade.

Animals

Specific pathogen free (SPF) grade male Sprague-Dawley rats (250 ± 20) g were provided by the Experimental Animal Center of Zhengzhou University (Zhengzhou, China). These rats were kept in a designated animal room at constant temperature (22 ± 2) ºC and humidity (50 ± 20) % with 12 h of light/dark per day and free access to water and food. All protocols of animal experiments were approved in accordance with the Regulations of Experimental Animal Administration issued by the Animal Ethics Committee of the First Affiliated Hospital of Zhengzhou University. Prior to the experiments, the rats were fasted for 12 h but with free access to water. After study use, the rats were euthanized with CO_2 gas.

Sample preparation

Each plasma sample (50 μL) was transferred to a 1.5-mL polypropylene tube containing 50 μL of internal standard (IS) solution (including 20 nM olanzapine-d3 and 1000 nM mycophenolic acid-d3) and 50 μL of methanol. The mixture was vortex mixed for 30 s, and then 150 μL methanol was precipitated. The tubes were vortex mixed vigorously for 1 min and centrifuged at 13800 *g* for 10 min at 4 ºC. Finally, 4 μL aliquots of the supernatant was injected into the UHPLC/TQD-MS system. Similarly, rat urine (50 μL) and bile (50 μL) samples were precipitated with methanol at a volumetric sample-to-methanol ratio of 1:3; after centrifugation, the resulting supernatants were applied for analysis. All the biological samples were stored at -80 °C.

Preparation of standard solutions and quality control samples

An appropriate amount of each authentic standard was separately dissolved with 60% methanol-water in a 10 mL volumetric flask to prepare the standard solution. Furthermore, an appropriate volume of each standard solution was

transferred into a 10 mL volumetric flask to the desired concentration as the stock solution. The mixed IS solution contained olanzapine-d3 and mycophenolic acid-d3 at final concentration of 20 nM and 1000 nM, respectively. All the solutions were stored at 4 ºC.

Calibration standard samples were prepared by spiking 50 μL blank plasma (or other biological samples) with 50 μL working solutions and 50 μL IS solution. Therefore, the plasma concentration ranges were 10-1000 nM for matrine (**A1**), 10-1000 nM for oxysophocarpine (**A2**), 40-4000 nM for oxymatrine (**A3**), 40-4000 nM for astragaloside IV (**B2**), 10-1000 nM for astragaloside III (**B3**), 10-1000 nM for ginsenoside Rh1 (**C1**), 10-1000 nM for notoginsenoside R2 (**C3**), 10-1000 nM for ginsenoside Rg2 (**C5**), 20-2000 nM for ginsenoside Rg1 (**C6**), 10-1000 nM for ginsenoside Rf (**C7**), 10-1000 nM for notoginsenoside R1 (**C8**), 20-2000 nM for ginsenoside Re (**C9**), 10-1000 nM for ginsenoside Rd (**D2**), 10-1000 nM for ginsenoside Rc (**D3**), 10-1000 nM for ginsenoside Rb2 (**D4**), 10-1000 nM for ginsenoside Rb1 (**D5**), respectively. Quality control (QC) samples were independently prepared in the same way at 2, 10, 40 times of LLOQ of each analyte. The calibration standard and QC samples were processed on each analysis day with the same procedures for plasma samples.

Chromatographic and mass spectrometric conditions

Ultra-high-performance liquid chromatography (UHPLC) analysis was performed on a Waters Acquity UHPLC I-Class system (Manchester, UK) for the quantitative analysis of Kang-Ai injection. Chromatographic separation was achieved on an BEH C18 column (2.1 × 50 mm, 1.7 μm) with water (A) and acetonitrile (**B**) (both including 0.1% formic acid) at a flow rate of 0.45 mL/min with column temperature of 35 ºC. The gradient flow profile was optimized as follows: 10% **B** from 0 to 0.5 min, 10-20% **B** from 0.5 to 1.5 min, maintaining 20% **B** from 1.5 to 4.5 min, 20-30% **B** from 4.5 to 5.5 min, 30-35% **B** from 5.5 to 7.5 min, 35-90% **B** from 7.5 to 9.5 min, keeping 90% **B** from 9.5 to 10.5 min, 90-10% **B** from 10.5 to 11.0 min, and maintaining 10% **B** from 11 to 12 min.

UHPLC system was coupled to a triple quadrupole mass spectrometer (Waters Xevo TQD, Waters, Manchester, UK). The detailed mass spectrometers were adjusted as follows: capillary voltage, 3.5 kV (ESI+) or 1.5 kV (ESI-); cone voltage, 50 V (ESI+) or 50 V (ESI-); source temperature, 350 ºC; desolvation gas flow, 650 L/h; The mass spectrometer was performed in the multiple reaction monitoring mode (MRM) using both positive and negative ionization. The quantitative parameters in MRM modes were same as our previous study. All experimental data were collected and processed using a Quanlynx software in Masslynx 4.1 platform.

Method validation

The developed UHPLC-MS/MS method was validated according to the Guidance for Industry: bioanalytical method validation from the US FDA for specificity, linearity, LLOQ, extraction recovery, matrix effects, precision, accuracy, stability and dilution integrity [23]. The assay validation of each analyte in rat biological samples including plasma, urine and bile were all performed based on the standard specification above.

Specificity was determined by comparing the chromatograms of blank samples (from six individual rats), with dosed samples after an intravenous bolus of Kang-Ai injection, and blank samples spiked with each analyte at LLOQ and IS. The calibration curves were constructed by the peak area ratios of the analytes to IS (Y), *versus* respective sample concentrations (X) applying a weighted ($1/x^2$) least squares linear regression analysis. LLOQ was determined based on the lowest concentrations for which acceptable linearity, accuracy and precision were demonstrated. The accuracies (the relative error, RE) and inter/intra-day precisions (the relative standard deviation, RSD) of the assay were evaluated by determining six replicates of QC samples (at low, middle and high concentrations) on three consecutive days.

Extraction recoveries (ER) and matrix effects (ME) were evaluated by a published experimental protocol [24]. The response of extracted QC sample was defined as A1. In addition, A2 referred to the corresponding standard solutions added into the post-extracted supernatant from biological matrix, while A3 corresponded to the responses of each analyte at three QC levels. The ER and ME values were calculated as follows: ER% = A1/A2 × 100%, and ME% = A2/A3 × 100%.

Stability tests were investigated at three QC levels under different conditions, including short-term stability (8 h exposure at room temperature), autosampler storage stability of the methanol-treated samples (at 8 °C for 18 h), freeze/thaw stability (three -80 °C ↔ 23 °C cycles), long-term stability (14 days storage at -80 °C). The dilution integrity was investigated by analyzing six replicate samples with each analyte, and each analyte were diluted 10-fold with blank rat matrix. Furthermore, the diluted samples were analyzed using freshly prepared calibration curve to calculate RE and RSD, which should be no more than ±15% as criterion.

In vivo rat studies

The rats in this study all received a single 30-minute intravenous infusion of Kang-Ai injection *via* the tail veins using TYD01-02 infusion pumps (Lead Fluid, Baoding, China). The dose was derived from the label daily dose of Kang-Ai injection (60 mL/person, once daily) according to dose normalization by body surface area [25]. For plasma pharmacokinetic studies, the rats were randomly received a single intravenous 30 min-bolus dose at 6 mL/kg. Blood samples (100 μL) were collected from the rats' external jugular veins into heparinized polypropylene tubes at 5, 15, 30, 45 min, and 1, 1.5, 2, 3, 4, 6, 8, 12 h). After gently shaking for 10 s, the blood samples were centrifuged at 13000 *g* for 10 min to yield plasma samples, which were kept frozen at -80 °C until analysis.

For urine sampling, the rats were housed singly in metabolic cages. And then, the urine samples were collected at 0-4, 4-8 and 8-12 h after starting infusion and were weighed. Likewise, bile samples were also collected at 0-3, 3-6, 6-9 and 9-12 h after starting infusion and were weighed. The urine and bile collection tubes were all frozen at -80 °C.

Protein binding assay

Binding of circulating alkaloids and saponins to rat plasma was measured by equilibrium dialysis using Spectra/Por 2 dialysis membranes (molecular weight cutoff, 12-14 kDa; Rancho Dominguez, CA, USA) as described [26]. After equilibrating for 24 h at 55 rpm and 37 °C, the dialysate and the plasma were sampled for analysis. In brief, the concentrations of each analyte in dialysate and rat plasma samples were determined for analysis after equilibrating at 55 rpm and 37 °C for 24 h. The concentrations of tested matrine, oxysophocarpine and oxymatrine were 2 μmol/L, while those of astragaloside IV, III, and ginsenosides Rh1, Rg2, Rg1, Rf, Re, Rd, Rc, Rb1, Rb2, notoginsenoside R1, R2, were 4 μmol/L. The unbound fraction ($f_{u\text{-}plasma}$) in rat plasma was calculated as follow: $f_{u\text{-}plasma} = C_d / C_p \times 100\%$, where the C_d and C_p values were the concentrations of each analyte in the dialysate sample and in the post-dialysis plasma sample, respectively.

Incubation systems

Phase I incubation system (100 μL) contained Tris-HCl buffer (50 mM, pH = 7.4), $MgCl_2$ (5 mM), each CYP isozyme, specific substrates, circulating compounds and NADPH (1 mM) as prescribed previously [18]. After incubation (37 °C, 60 min), the reaction was terminated by ice-cold acetonitrile (100 μL), following by centrifugation at 13800 *g* for 10 min. The supernatant (8 μL) was acquired for ultra-high-performance liquid chromatography (UHPLC) system (Waters, Manchester, UK) analysis.

For glucuronidation assays, the incubation system (100 μL) contained Tris-HCl buffer (50 mM, pH = 7.4), alamethicin (22 μg/mL), D-saccharic-1, 4-lactone (4.4 mM), each UGT enzyme, specific substrates, circulating compounds and UDPGA (3.5 mM) as described recently [18]. The reaction was terminated by ice-cold acetonitrile (100 μL) after incubation at 37 °C for 60 min. After centrifugation (13800 *g*, 10 min), the supernatant (8 μL) was obtained for determination by UHPLC system.

Analysis of inhibitory effects

In this study, phenacetin (100 μM), coumarin (100 μM), bupropion (100 μM), paclitaxel (60 μM), tolbutamide (200 μM), mephenytoin (100 μM), chlorzoxazone (200 μM) and nifedipine (40 μM) have been used as the probe substrates for CYP1A2, 2A6, 2B6, 2C8, 2C9, 2C19, 2E1 and 3A4, respectively [27]. The substrates were incubated with each CYP isozyme at different protein concentrations (0.05 mg/mL for CYP1A2 and 3A4; 0.1 mg/mL for CYP2A6, 2B6, 2C8, 2C9, 2C19 and 2E1) in the absence (control) and presence of different herbal compounds (1, 10, 100 and 1000 μM for matrine and oxymatrine; 0.1, 1, 10 and 100 μM for astragaloside and ginsenoside).

Similarly, β-estradiol (60 μM), propofol (40 μM) and 4-MU (350 μM) were typically used as the substrates for UGT1A1, 1A9 and 2B7, respectively [28]. The protein concentrations for UGT1A1, 1A9, and 2B7 were 0.125, 0.05, and 0.05 mg/mL, respectively. The concentrations were 1, 10, 100 and 1000 μM for matrine and oxymatrine, and 0.1, 1, 10 and 100 μM for astragaloside and ginsenoside based on the detailed plasma concentration after intravenous Kang-Ai injection.

The half-inhibition concentration (IC_{50}) values were determined by non-linear regression analysis. The inhibitory effects towards each CYP or UGT enzyme were divided into four categories as follows, potent (IC_{50} < 1 μM), moderate (1 μM < IC_{50} < 10 μM), weak (10 μM < IC_{50} < 100 μM), or no inhibition (IC_{50} > 100 μM) [18]. The inhibition mechanism towards corresponding CYP and UGT isoforms were further explored.

Inhibition kinetic analysis

The inhibition constant (K_i) values were obtained by multiple concentrations of substrates in the absence or presence of multiple concentrations of herbal compounds as described previously [18, 27, 28]. Competitive inhibition, noncompetitive inhibition, and mixed-type inhibition models were used to determine the K_i values by nonlinear regression analysis using the equation (1), equation (2) and equation (3), respectively. The model with the smallest Akaike information criterion (AIC) and Schwartz information criterion (SC) values was considered as the best model, following the obtained appropriate K_i values.

The detailed parameters for three equations were as follow. *V* is the velocity of the reaction. The [S] and [I] are the concentrations of substrate and herbal compounds, respectively. K_i is the constant describing the affinity between herbal compounds and the enzyme. K_m is the substrate concentration at half of the maximum velocity (V_{max}) of the reaction. The αKi describes the affinity of herbal compounds to the complex of enzyme and substrate; When α is very large (α >> 1), the binding of inhibitor would prevent the binding of substrate, and the mixed inhibition model becomes identical to competitive inhibition.

$$V = \frac{V_{max} \times [S]}{K_m \times (1 + \frac{[I]}{K_i}) + [S]} \quad (1)$$

$$V = \frac{V_{max} \times [S]}{(K_m + [S]) \times (1 + \frac{[I]}{K_i}} \quad (2)$$

$$V = \frac{V_{max} \times [S]}{K_m \times (1 + \frac{[I]}{K_i}) + [S] \times (1 + \frac{[I]}{\alpha K_i})} \quad (3)$$

Data processing

Pharmacokinetic parameters were estimated by non-compartmental analysis using WinNonlin 6.3 software (Pharsight, NC, US). Data are presented as the mean ± SD (n = 3). The area under the concentration-time curve up to the last measured point in time (AUC_{0-t}) was calculated using the trapezoidal rule. The total plasma clearance ($CL_{tot,\,p}$) was calculated by dividing the compound dose by the $AUC_{0-\infty}$, and the distribution volume at steady state (V_{SS}) was estimated by multiplying the $CL_{tot,\,p}$ by the mean residence time (MRT). The renal excretory clearance (CL_R) and hepatobiliary (CL_B) was determined by dividing the cumulative amount excreted into urine ($Cum.A_{e\text{-}U}$) and bile ($Cum.A_{e\text{-}B}$) by the plasma $AUC_{0-\infty}$, respectively. The fractions of dose excreted into urine ($f_{e\text{-}U}$) and the fractions of dose excreted into bile ($f_{e\text{-}B}$) were established using the relationship $Cum.A_{e\text{-}U}$/Dose and C$um.A_{e\text{-}B}$/Dose, respectively. Mean differences between treatment and control groups were analyzed by two-tailed unpaired Student's t test by Graphpad Prism V5 software (SanDiego, CA). The level of significance was set at $p < 0.05$ (∗), $p < 0.01$ (∗∗) or $p < 0.001$ (∗∗∗).

Results

Xenobiotics detected in rat samples

After dosing Kang-Ai injection to rats (6 mL/kg), a total of 9 circulating alkaloids, 6 astragalosides and 22 ginsenosides were detected and characterized in rat samples (Additional file 1: Fig. S1A & Table S1). Based on their individual content level from Kang-Ai injection [9], these compounds were graded into five dose levels (Additional file 1: Fig. S1B): Level I was over 1000 μg/mL for only oxymatrine (**A3**); Level II was between 100 and 1000 μg/mL for ginsenoside Rg1 (**C6**) and Re (**C9**); Level III was ranged from 10 to 100 μg/mL for matrine (**A1**), astragaloside IV (**B2**), notoginsenoside R2 (**C3**), ginsenoside Rg2 (**C5**), Rf (**C7**) and Rc (**D3**); Level IV was from 1 to 10 μg/mL for astragaloside III (**B3**), VI (**B4**), V (**B5**), notoginsenoside R1 (**C8**), ginsenoside Rh1 (**C1**), Rd (**D2**), Rb2 (**D4**), Rb1 (**D5**), Rh4 (**E2**), Rg6 (**E3**), F4 (**E4**); Level V was all less than 1 μg/mL for oxysophocarpine (**A2**), isoastragaloside IV (**B1**), ginsenoside F1 (**C2**), F3 (**C4**), F2 (**D1**), Rk3 (**E1**).

Plasma Pharmacokinetics Of Circulating Alkaloids And Saponins In Rats

Table 1 summarized the PK parameters of circulating alkaloids (**A1-A3**), astragalosides (**B2**, **B3**) and ginsenosides (**C1**, **C3**, **C5-C9**, **D2-D5**) from intravenously dosed Kang-Ai injection. Figure 1A displayed the total plasma concentrations of the alkaloids over time, during and after a 30-min intravenous infusion of Kang-Ai injection in rats. Clearly, the plasma C_{max} value of matrine (**A1**) were determined after stopping the infusion for 30 min. After the 30-min infusion, its plasma concentration increased with mean $t_{1/2}$ values of 4.33 h. In addition, the C_{max} values of oxysophocarpine (**A2**) and oxymatrine (**A3**) were both measured just before stopping the infusion, following the declined plasma concentration with shorter $t_{1/2}$ values of 1.78 and 2.73 h, respectively. The mean V_{SS} values of **A1**, **A2** and **A3** were 9.85, 25.20 and 220.11 mL/kg, respectively, suggesting these three alkaloids all had small V_d values. Besides, the $CL_{tot,\,p}$ values of **A3** was 111.34 mL/h/kg and those of **A1** and **A2** were 1.58 and 12.31, respectively, indicating that **A3** and **A1**, **A2** had moderate and low total clearance, respectively. Furthermore, these circulating alkaloids (**A1-A3**) were not extensively bound with $f_{u-plasma}$ values over 90%.

Table 1
Pharmacokinetic parameters of circulating alkaloids and saponins in rats after receiving a 30-min infusion of Kang-Ai injection at 6 mL/kg.

ID	$t_{1/2}$	C_{max}	AUC_{0-12h}	$CL_{tot,p}$	V_{SS}	$f_{e-B,0-12h}$	CL_B	$f_{e-U,0-12h}$	CL_R	$f_{u-plasma}$
	h	nmol/L	nmol/L*h	mL/h	mL	(%)	mL/h	(%)	mL/h	(%)
A1#	4.33 ± 2.18	15.06 ± 3.58	68.61 ± 9.85	1.58 ± 0.36	9.85 ± 2.47	36.55 ± 4.24	0.57 ± 0.09	57.40 ± 4.88	0.90 ± 0.17	92.67 ± 6.81
A2	1.78 ± 1.55	169.87 ± 27.36	257.67 ± 30.97	12.31 ± 1.62	25.20 ± 14.82	51.92 ± 8.98	6.34 ± 1.21	38.60 ± 11.22	4.75 ± 1.53	91.15 ± 4.95
A3#	2.73 ± 1.16	422.70 ± 55.50	502.71 ± 93.02	111.34 ± 18.49	220.11 ± 53.82	28.96 ± 3.69	31.95 ± 4.76	63.83 ± 2.28	70.85 ± 10.40	93.24 ± 6.52
B1	—	—	—	—	—	30.40 ± 3.79	—	—	—	—
B2	1.64 ± 0.26	2363.99 ± 251.85	4523.65 ± 464.66	28.39 ± 2.85	64.88 ± 10.23	8.79 ± 1.29	2.49 ± 0.35	17.12 ± 3.13	4.84 ± 0.84	12.35 ± 1.02
B3	0.33 ± 0.13	54.75 ± 10.23	34.29 ± 5.22	206.96 ± 36.55	91.99 ± 21.98	32.61 ± 3.00	67.06 ± 10.52	2.60 ± 0.69	5.25 ± 1.10	11.04 ± 0.86
B4	—	—	—	—	—	—	—	63.43 ± 11.75	—	—
B5	—	—	—	—	—	—	—	51.36 ± 7.44	—	—
C1	0.44 ± 0.39	140.43 ± 20.40	91.16 ± 4.77	198.38 ± 16.38	93.62 ± 45.64	9.71 ± 0.98	19.27 ± 2.44	9.59 ± 1.68	18.97 ± 3.34	46.32 ± 5.03
C2	—	—	—	—	—	24.20 ± 4.93	—	23.37 ± 7.94	—	—
C3	0.29 ± 0.12	128.03 ± 13.27	85.57 ± 10.54	255.80 ± 34.97	99.30 ± 20.42	23.55 ± 1.97	59.94 ± 6.71	10.27 ± 2.49	25.62 ± 3.48	35.24 ± 2.85
C4	—	—	—	—	—	67.93 ± 8.80	—	24.46 ± 3.37	—	—
C5	9.77 ± 13.75	230.90 ± 17.45	192.29 ± 42.13	157.78 ± 74.80	791.61 ± 713.90	20.76 ± 3.37	30.75 ± 17.04	2.23 ± 0.61	3.31 ± 1.86	26.54 ± 3.28
C6	1.20 ± 1.23	1565.45 ± 174.98	1517.34 ± 263.46	156.65 ± 30.66	144.15 ± 64.23	20.71 ± 3.62	33.27 ± 12.03	39.79 ± 5.88	62.25 ± 14.38	86.35 ± 7.32
C7	0.63 ± 0.31	943.15 ± 171.83	674.18 ± 89.61	109.50 ± 15.38	50.05 ± 7.85	13.12 ± 1.68	14.48 ± 3.46	17.77 ± 3.90	19.33 ± 4.45	60.23 ± 7.01

Note: # means the units of C_{max} and AUC_{0-12h} for matrine and oxymatrine are μmol/L and μmol/L*h, respectively. See Table S1 for the compounds' ID and names.

ID	$t_{1/2}$	C_{max}	AUC_{0-12h}	$CL_{tot,p}$	V_{SS}	$f_{e-B,0-12h}$	CL_B	$f_{e-U,0-12h}$	CL_R	$f_{u-plasma}$
	h	nmol/L	nmol/L*h	mL/h	mL	(%)	mL/h	(%)	mL/h	(%)
C8	0.75 ± 0.16	121.07 ± 21.08	133.10 ± 17.03	72.70 ± 6.63	71.71 ± 14.31	12.00 ± 1.57	8.73 ± 1.49	72.12 ± 13.01	51.84 ± 5.77	90.36 ± 4.22
C9	1.07 ± 0.84	1338.77 ± 88.07	1000.55 ± 62.12	156.32 ± 11.64	100.55 ± 26.96	28.27 ± 4.16	44.03 ± 5.77	29.54 ± 6.03	46.03 ± 9.04	87.36 ± 6.59
D1	—	—	—	—	—	7.46 ± 2.11	—	—	—	—
D2	5.84 ± 3.13	766.17 ± 57.86	1696.75 ± 124.20	5.83 ± 0.67	35.69 ± 11.39	5.55 ± 1.02	0.33 ± 0.08	19.00 ± 5.33	1.11 ± 0.32	0.75 ± 0.08
D3	6.29 ± 3.17	877.14 ± 39.49	2165.94 ± 186.38	5.60 ± 1.41	37.81 ± 10.15	—	—	10.48 ± 1.31	0.58 ± 0.15	1.12 ± 0.12
D4	4.12 ± 0.83	301.33 ± 34.23	698.17 ± 105.74	7.80 ± 1.14	39.58 ± 7.30	—	—	27.80 ± 4.47	2.14 ± 0.27	0.67 ± 0.05
D5	7.22 ± 7.03	497.21 ± 75.11	1536.70 ± 223.18	6.16 ± 1.57	46.96 ± 19.87	—	—	6.41 ± 1.47	0.38 ± 0.09	0.96 ± 0.09
E1	—	—	—	—	—	27.80 ± 7.01	—	—	—	—
E2	—	—	—	—	—	46.95 ± 6.46	—	—	—	—
E3	—	—	—	—	—	31.31 ± 6.25	—	—	—	—
E4	—	—	—	—	—	29.36 ± 3.14	—	—	—	—
A4	—	—	—	—	—	11.14 ± 1.05	—	42.80 ± 14.69	—	—
A5	2.15 ± 0.50	264.42 ± 47.19	380.06 ± 117.01	26.77 ± 11.13	55.47 ± 6.92	10.30 ± 1.11	2.68 ± 0.82	37.56 ± 15.13	10.99 ± 8.12	—
A6	2.16 ± 1.28	344.22 ± 40.74	509.97 ± 93.65	47.70 ± 10.72	93.63 ± 24.86	12.50 ± 1.32	5.86 ± 1.10	12.92 ± 4.98	6.23 ± 2.97	—
A7	5.73 ± 1.74	202.37 ± 19.05	777.15 ± 81.47	20.03 ± 4.84	150.70 ± 19.02	7.30 ± 1.41	1.42 ± 0.17	61.05 ± 10.61	12.32 ± 4.14	—
A8	2.32 ± 1.03	421.27 ± 68.11	567.07 ± 114.95	7.93 ± 1.77	16.89 ± 5.16	34.12 ± 4.23	2.67 ± 0.46	15.28 ± 5.11	1.23 ± 0.50	—

Note: # means the units of C_{max} and AUC_{0-12h} for matrine and oxymatrine are μmol/L and μmol/L*h, respectively. See Table S1 for the compounds' ID and names.

ID	$t_{1/2}$	C_{max}	AUC_{0-12h}	$CL_{tot,p}$	V_{SS}	$f_{e-B,0-12h}$	CL_B	$f_{e-U,0-12h}$	CL_R	$f_{u-plasma}$
	h	nmol/L	nmol/L*h	mL/h	mL	(%)	mL/h	(%)	mL/h	(%)
A9	0.82 ± 0.37	396.86 ± 49.71	486.66 ± 132.17	56.05 ± 22.70	53.50 ± 7.71	1.27 ± 0.20	0.68 ± 0.16	59.77 ± 8.80	34.24 ± 17.17	—
B6	—	—	—	—	—	—	—	74.96 ± 6.01	—	—
C10	—	—	—	—	—	—	—	40.28 ± 5.48	—	—
C11	—	—	—	—	—	—	—	48.30 ± 10.27	—	—
C12	—	—	—	—	—	—	—	36.16 ± 7.04	—	—
C13	—	—	—	—	—	—	—	38.72 ± 6.57	—	—

Note: # means the units of C_{max} and AUC_{0-12h} for matrine and oxymatrine are μmol/L and μmol/L*h, respectively. See Table S1 for the compounds' ID and names.

The plasma concentration-time curves and PK parameters of astragaloside IV (**B2**) and III (**B3**) were shown in Fig. 1B & Table 1, respectively. The plasma C_{max} (2363.99 nmol/L) and $AUC_{0-\infty}$ (4523.65 nmol/L*h) values of **B2** were far higher than those of **B3** with C_{max} and $AUC_{0-\infty}$ values of (54.75 nmol/L) and $AUC_{0-\infty}$ (34.29 nmol/L*h), due to the differences in the compounds' doses from the injection. Besides, the $t_{1/2}$ values of these two astragalosides were both small and less than 2 h. Similarly, **B2** and **B3** both exhibited the small V_d values (< 100 mL/kg), whereas **B2** (28.39 mL/h/kg) and **B3** (206.96 mL/h/kg) had low and moderate total clearance, respectively. Protein binding assay demonstrated that **B2** and **B3** were extensively bound in rat plasma (nearly 90%).

These circulating ginsenosides in plasma could be classified into two categories, PPT-type ginsenosides (**C1**, **C3**, **C5-C9**) and PPD-type ginsenosides (**D2-D5**). Figures 1C & 1D summarized the plasma concentrations of the PPT-type ginsenosides and PPD-type ginsenosides over time, respectively. It was notably shown that the T_{max} values of PPT-type ginsenosides were 30 min, whereas those of PPD-type ginsenosides were measured after stopping infusion for 15 min. In addition, the C_{4h} values of the PPT-type ginsenosides were very low, while those of the PPD-type ginsenosides still maintained a moderate plasma concentration. These suggested that the PPT-type ginsenosides possessed the longer MRT, and were eliminated more quickly than PPD-type ginsenosides. Another strong evidence was that $CL_{tot,p}$ values of PPT-type ginsenosides (72.70-255.80 mL/h/kg) were approximately 10 times of those of PPT-type ginsenosides (5.60–7.80 mL/h/kg). Besides, except for ginsenoside Rg2 (**C5**) about the $t_{1/2}$ value of 9.77 h, the PPT-type ginsenosides exhibited the shorter elimination half-lives values of i.e., 0.29–1.20 h for ginsenoside Rh1 (**C1**), Rg1 (**C6**), Rf (**C7**), Re (**C9**) and notoginsenoside R1 (**C8**), R2 (**C3**) than those of 4.12–7.22 h for ginsenoside Rd (**D2**), Rc (**D3**), Rb2 (**D4**) and Rb1 (**D5**). The V_{SS} values of PPT-type ginsenosides and PPD-type ginsenosides were 50.05-791.61 and 35.69–46.96 mL/kg, respectively, indicating that the PPT-type ginsenosides were more easily distributed in various body fluids and tissues than the PPD-type ginsenosides. Additionally, the PPT-type ginsenosides (**C1**, **C3**, **C5-C9**) were not significantly bound, whereas the PPD-type ginsenosides (**D2-D5**) were obviously bound (around 99%) in rat plasma.

Moreover, due to lack of the available authentic standards, virtual quantification of other main circulating herbal compounds in rat plasma, including baptifoline (**A5**), 9α-hydroxy-sophocarpine (**A6**), leontalbinine N-oxide (**A7**),

mamanine (**A8**), sophoranol (**A9**), were achieved using the calibration curve of an available reference standard of an analog that bore close structural similarity to the analyte. Figure 1E & Table 1 showed their mean plasma concentration-time curves and calculated relative PK parameters, respectively. The C_{max} values ranged from 202.37-421.27 nmol/L, and the T_{max} values were all determined just before stopping the infusion. Besides, **A7** exhibited the longest MRT (7.94 h) and $t_{1/2}$ (5.73 h) values among these five alkaloids. The small V_{SS} (16.89–150.70 mL/kg) and $CL_{tot,p}$ (7.93–56.05 mL/h/kg) values indicated that these alkaloids were slowly distributed in various body fluids and tissues, and slowly cleared from the systemic circulation.

To better demonstrate the systemic exposure in rat plasma, the comparison of the AUC_{0-12h} values of circulation alkaloids and saponins were displayed in Fig. 2A. Obviously, oxymatrine (**A3**) exhibited the most abundant exposure with 502.71 μmol/L*h, due to the most abundant dose level from Kang-Ai injection. Additionally, **A1**, **B2**, **D3**, **D2**, **D5**, **C6**, **C9**, **A7**, **D4**, **C7**, **A8**, **A6**, **A9**, **A5**, **A2**, **C5**, **C8**, in descending order, exhibited substantially higher total levels of plasma exposure with the AUC_{0-12h} values over 100 nmol/L*h, whereas the levels of plasma exposure to other compounds (**B3**, **C1**, **C3**) were quite low, due to their low compound dose from Kang-Ai injection.

Urinary and biliary excretion of circulating alkaloids and saponins in rats

Table 1 summarized the urinary and biliary excretion parameters of circulating alkaloids and saponins. Meanwhile, Figs. 2B & 2C showed their cumulative excretion amounts in urine and bile, respectively. For the circulating alkaloids (**A1-A3**), the renal and hepatobiliary excretion of the unchanged compounds represented the major routes of elimination (Table 1). This was attributed that **A1** (57.40%), **A2** (38.60%) and **A3** (63.83%) exhibited an extraordinarily high $f_{e-U,0-12h}$ values, the sum of which with the $f_{e-B,0-12h}$ values (36.55%, 51.92%, 28.96%, respectively) exceeded 90% of individual dose levels.

Astragaloside III (**B3**) was eliminated more extensively *via* hepatobiliary excretion (f_{e-B}, 67.06%) than renal excretion (f_{e-U}, 5.25%) (Table 1). Unlike for **B3**, renal excretion was a minor elimination pathway for astragaloside IV (**B2**) (f_{e-U}, 4.84%), and the same fact was that the fraction of dosed **B2** was excreted into bile (f_{e-B}) about 2.49%.

The PPT-type ginsenosides (**C1-C9**), except ginsenoside Rg2 (**C5**), all exhibited the large f_{e-U} values (9.59%-72.17%) (Table 1), suggesting that the renal excretion was the predominant elimination route responsible for their systemic clearance. Similarly, the PPD-type ginsenosides (**D2-D5**), exhibited moderate f_{e-U} values (6.41%-27.8%), which was around a half of the values of PPT-type ginsenosides. In addition, in rat bile, the PPT-type ginsenosides were the most abundant herbal compounds with f_{e-B} values of 9.71%-67.93%, whereas only two PPD-type ginsenosides, ginsenoside F2 (**D1**) and Rd (**D2**) could be detected and displayed the small f_{e-B} values of 7.46% and 5.55%, respectively. Consistent with the inter-compound differences in $CL_{tot,p}$ values, the CL_R and CL_B values for these PPT-type ginsenosides (**C1-C9**) were significantly greater than those respect values for the PPD-type ginsenosides (**D1-D5**).

Moreover, other alkaloids (**A4-A9**) were eliminated more extensively unchanged *via* the renal excretion (f_{e-U}, 12.92%-61.05%) than the hepatobiliary excretion (f_{e-B}, 1.27%-34.12%) (Table 1). The CL_R and CL_B values for the alkaloids (**A4-A9**) kept in line with their $CL_{tot,p}$ values. Another astragaloside, astragaloside VII (**B6**) was excreted 74.96% of the dose derived from Kang-Ai injection to urine. Another four PPT-type ginsenosides, ginsenoside R1 (**C10**), Re4 (**C11**), notoginsenoside R3 (**C12**) and 20-gluco-ginsenoside Rf (**C13**) were all subjected to be eliminated by the renal excretion with f_{e-U} values of 36.16%-48.30%, whereas their hepatobiliary excretion appeared to be negligible.

Inhibitory effects of herbal compounds towards each CYP and UGT isozyme

Based on Table 1, matrine (**A1**), oxymatrine (**A3**), astragaloside IV (**B2**), ginsenoside Rg1 (**C6**), Rf (**C7**), Re (**C9**), Rd (**D2**), Rc (**D3**), Rb1 (**D5**) exhibited the C_{max} values about or over 0.5 μmol/L after intravenous Kang-Ai injection. Therefore, these nine major circulating compounds were selected to evaluate the inhibitory effects toward several common CYP and UGT enzymes. As shown in Fig. 3, A1 (1000 μM) displayed inhibitory effects against CYP3A4 (46.52%), whereas **A3** (1000 μM) could inhibit the metabolic activity of CYP2A6 (75.36%), 2C19 (70.42%), 2E1 (76.52%), 3A4 (53.97%). In addition, **B2** (100 μM) exhibited inhibitory activity towards CYP2C9 (52.36%). Besides, *PPT-type* ginsenosides, **C6** (100 μM) and **C9** (100 μM) mainly inhibited the function of UGT1A1 (53.26%) and CYP2C8 (30.25%), respectively, while almost no changes were observed for **C7** (100 μM) against these CYP and UGT enzymes. Furthermore, **D2** (100 μM) exhibited inhibition on the metabolic activity of CYP2B6 (30.36%) and 3A4 (42.36%), whereas **D3** (100 μM) and **D5** (100 μM) showed inhibitory effects on UGT1A9 (30.26%) and CYP2C9 (15.36%), respectively.

Moreover, the inhibition data (Fig. 4) were fit to log (I) and normalized response equations to obtain the IC_{50} values. The inhibition trend of the abundant compounds towards these CYP and UGT enzymes showed in a dose dependent manner, and their IC_{50} values were 387.40 (**A1** against CYP3A4), 604.60 (**A3** against CYP3A4), 65.00 (**B2** towards CYP2C9), 92.21 (**C6** against UGT1A1), 24.03 (**C9** towards CYP2C8), 20.19 (**D2** against CYP2B6), 40.96 (**D2** towards CYP3A4), 28.96 (**D3** against UGT1A9) and 8.81 μM (**D5** towards CYP2C9), respectively (Additional file 1: Table S8). The inhibition mechanism was further evaluated based on three inhibition kinetic models.

Analysis Of Inhibition Mechanism

The AIC and SC values (Table 2) were obtained after the inhibition data were modeled by three conventional inhibition equation (i.e., competitive, noncompetitive and mixed-type). Based on the smallest AIC and SC values principle, **C6** displayed competitive inhibition against UGT1A1, while **C9** exhibited mixed-type inhibition against CYP2C8. Noncompetitive inhibition kinetics were observed for **A1** against CYP3A4, **A3** towards CYP3A4, **B2** against CYP2C9, **D2** towards CYP2B6 and 3A4, **D3** against UGT1A9 and **D5** towards CYP2C9.

Table 2
Inhibition parameters of circulating alkaloids and saponins against several CYP and UGT isozymes. Data represent the mean ± standard deviation of triplicate.

Compounds	Isozymes	Inhibition type	K_i (μM)	α	R^2	AICs	SCs	Selection	C_{max}/K_i
Matrine (A1)	CYP3A4	Competitive	122.2 ± 27.4	——	0.9945	-25.7	-22.7		
		Noncompetitive	**420.7 ± 30.9**	**——**	**0.9822**	**-49.8**	**-46.8**	**√**	**0.04**
		Mixed-type	443.6 ± 152.5	0.9 ± 0.5	0.9822	-47.8	-43.8		
Oxymatrine (A3)	CYP3A4	Competitive	113.3 ± 19.1	——	0.9650	-41.8	-38.8		
		Noncompetitive	**367.6 ± 23.8**	**——**	**0.9870**	**-61.5**	**-58.5**	**√**	**1.15**
		Mixed-type	287.4 ± 70.3	1.5 ± 0.7	0.9877	-60.6	-56.6		
Astragaloside IV (B2)	CYP2C9	Competitive	17.4 ± 3.7	——	0.9480	-113.3	-110.3		
		Noncompetitive	**55.8 ± 5.3**	**——**	**0.9708**	**-124.8**	**-121.8**	**√**	**0.04**
		Mixed-type	45.0 ± 16.6	1.5 ± 1.0	0.9713	-123.1	-119.2		
Ginsenoside Rg1 (C6)	UGT1A1	Competitive	140.6 ± 10.5	——	0.9952	176.4	179.4	√	0.01
		Noncompetitive	187.2 ± 12.7	——	0.9943	179.8	182.8		
		Mixed-type	147.3 ± 29.9	8.3 ± 37.2	0.9952	178.7	182.7		
Ginsenoside Re (C9)	CYP2C8	Competitive	8.2 ± 1.1	——	0.9790	-121.3	-118.3		
		Noncompetitive	26.5 ± 2.2	——	0.9793	-121.6	-118.6		
		Mixed-type	13.3 ± 2.9	4.2 ± 2.3	0.9862	-127.8	-123.8	√	0.1
Ginsenoside Rd (D2)	CYP2B6	Competitive	10.2 ± 2.1	——	0.9484	19.4	22.4		
		Noncompetitive	**37.2 ± 2.3**	**——**	**0.9877**	**-9.2**	**-6.2**	**√**	**0.02**

Note: C_{max}/K_i also named $[I]/K_i$ standard ($[I]/Ki < 0.1$, low possibility DDI; $1 > [I]/Ki > 0.1$, medium possibility DDI; $[I]/Ki > 1$, high possibility DDI).

Compounds	Isozymes	Inhibition type	K_i (μM)	α	R^2	AICs	SCs	Selection	C_{max}/K_i
		Mixed-type	36.3 ± 10.2	1.0 ± 0.4	0.9877	-7.2	-3.2		
Ginsenoside Rd (D2)	CYP3A4	Competitive	8.7 ± 2.3	——	0.9226	-31.9	-28.9		
		Noncompetitive	**32.8 ± 2.2**	**——**	**0.9846**	**-64.2**	**-61.2**	√	**0.02**
		Mixed-type	44.2 ± 16.2	0.6 ± 0.3	0.9854	-63.3	-59.3		
Ginsenoside Rc (D3)	UGT1A9	Competitive	8.9 ± 1.5	——	0.9634	122.8	125.8		
		Noncompetitive	**22.3 ± 1.4**	**——**	**0.9877**	**100.9**	**103.9**	√	**0.04**
		Mixed-type	27.0 ± 7.5	0.7 ± 0.3	0.9881	102.3	106.3		
Ginsenoside Rb1 (D5)	CYP2C9	Competitive	8.2 ± 1.0	——	0.9812	-115.9	-112.9		
		Noncompetitive	**16.1 ± 0.9**	**——**	**0.9921**	**-133.2**	**-130.3**	√	**0.03**
		Mixed-type	18.8 ± 4.3	0.7 ± 0.3	0.9923	-131.8	-127.9		

Note: C_{max}/K_i also named $[I]/K_i$ standard ($[I]/Ki < 0.1$, low possibility DDI; $1 > [I]/Ki > 0.1$, medium possibility DDI; $[I]/Ki > 1$, high possibility DDI).

Furthermore, the Dixon plots for **A1** against CYP3A4 (Fig. 5A), **A3** towards CYP3A4 (Fig. 5B), **B2** against CYP2C9 (Fig. 5C), **C6** towards UGT1A1 (Fig. 5D), **C9** against CYP2C8 (Fig. 5E), **D2** towards CYP2B6 (Fig. 5F) and 3A4 (Fig. 5G), **D3** against UGT1A9 (Fig. 5H) and **D5** towards CYP2C9 (Fig. 5I) also provided strong evidences to support this judgment about the inhibition mechanism. Their respective K_i values were 420.7, 367.6, 55.8, 140.6, 13.3, 37.2, 32.8, 22.3 and 16.1 μM (Table 2). These findings suggested that the major circulating compounds have weak or no inhibition on the metabolic activity of common CYP and UGT enzymes with K_i values all over 10 μM.

Potential DDI risks

Based on the $[I]/K_i$ values *in vitro*, potential DDI risks *in vivo* could be predicted [27, 28]. Traditionally, $[I]/Ki < 0.1$, low possibility DDI; $1 > [I]/Ki > 0.1$, medium possibility DDI; $[I]/Ki > 1$, high possibility DDI [18]. In this study, the $[I]/K_i$ value for oxymatrine (**A3**) against CYP3A4 was 1.15, whereas other $[I]/K_i$ values were all no more than 0.1 (Table 2). Therefore, it seemed more possible to trigger DDI when Kang-Ai injection were co-administrated with clinical drugs which were metabolized by CYP3A4. This was mainly attributed to the abundant exposure of **A3**.

Discussion

Bioactive compounds with adequate abundance in herbal injection and favorable PK properties are mostly believed to be responsible for the pharmacological effects and therapeutic efficacy [4]. In the current study, alkaloids and saponins

derived from Kang-Ai injection are two classes of bioactive compounds which are likely responsible for the adjuvant therapy of many cancers (Additional file 1: Table S1) [6, 8]. After dosing, oxymatrine (**A3**), matrine (**A1**), astragaloside IV (**B2**), ginsenosides Rc (**D3**), Rd (**D2**), Rb1 (**D5**), Rg1 (**C6**) and Re (**C9**), all exhibited considerably high levels of systemic exposure (over 1000 nmol/L*h) (Fig. 2A), indicating that these circulating compounds are worth special consideration in the pharmacological research. Besides, the abundant exposure of **A1** may be attributed the metabolism of **A3** by CYP3As [29]. In addition, the considerable systemic exposure for **A3**, **A1**, **D3**, **D2** and **D5**, seemed to be correlated with the significantly longer $t_{1/2}$ values of 2.73–7.22 hour than those of **B2**, **C6** and **C9** (1.07–1.64 hour) (Table 1). This phenomenon that long elimination half-life could significantly counterbalance influence on systemic exposure to herbal compounds with poor bioavailability has been proved previously [30].

Except the systemic exposure of major circulating compounds, we also investigate their elimination in the current study (Table 1). After dosing Kang-Ai injection, oxymatrine (**A3**) and matrine (**A1**) mainly involved in the renal and hepatobiliary excretion of the parent compounds (over 90%), of which parts of circulated **A1** was originated from the metabolism of **A3** by CYP3A4 [11]. Only about 25% of dosed astragaloside IV (**B2**) were detected as parent compound in urine and bile, and this was probably attributed to the de-glycosylation of **B2** to its sapogenin [15]. Additionally, ginsenosides Rg1 (**C6**) and Re (**C9**) were eliminated mainly to urine and bile (nearly 60%), whereas it proved that approximately 25% of ginsenoside Rd (**D2**) was excreted *via* renal and hepatobiliary elimination. Ginsenosides Rc (**D3**) and Rb1 (**D5**) were not detected in bile, and mainly were eliminated through renal excretion. Except the *in vivo* metabolism, i.e., oxidation and de-glycosylation [16], the delivery to the rat tissues of circulating herbal compounds through blood flow were also an important factor to determine the systemic exposure and excretion of circulating compounds [31]. The V_{SS} values of dosed **A3**, **C6** and **C9** were 100.55-220.11 mL/kg, which were near the rat extracellular volume (300 mL/kg) [32], indicating that these herbal compounds could be distributed evenly in various body tissues, except several barriered tissues. However, this elimination route warrant future investigation.

In addition, the obtained PK parameters (Table 1) also could enable us to compare the plasma concentrations of the alkaloids and saponins with the reported effective concentrations (IC_{50} or EC_{50} values) for pharmacological activities. Oxymatrine (**A3**) exhibited the most abundant concentration (422.70 μmol/L) after dosing Kang-Ai injection, which is still obviously below the reported effective concentrations (473.48-3787.84 μmol/L) for several tumor cell lines, including HepG2, MCF-7, HeLa, A549 cells [33]. However, for SW-620, BGC823, A375 cells, **A3** is sufficiently effective to inhibit the tumor cell viability (0.10–40.00 μmol/L) [33]. Similar results were obtained for matrine (**A1**) and its derivatives [34], astragaloside IV (**B2**) [35], and several main ginsenosides [36]. Although the low plasma concentrations do not result in the ineffectiveness of Kang-Ai injection for the therapeutic effects, they may limit the contribution of bioactive compounds to the current adjuvant therapy. How to achieve the higher plasma concentrations is an important idea to develop new and superior adjuvant agents derived from the current Kang-Ai injection.

Kang-Ai injection are the combinations of two herbs and Kushensu, of which complex chemical compositions increased the DDI risks. Usually, the induction and inhibition of CYP and UGT enzymes can facilitate the metabolism and elimination of their drug substrates and caused unexpected adverse effect. Previously, oxymatrine (**A3**) was subjected to be metabolized to matrine (**A1**) rapidly in pooled HLM (K_m = 220.78 μM) and HIM (K_m = 150.22 μM), and CYP3A4 (K_m = 341.35 μM) isozyme greatly contributed to this transformation [37]. However, **A1** could not be extensively metabolized by CYPs and UGTs [38]. The [I]/K_i value for oxymatrine (**A3**) against CYP3A4 was 1.15 seemed more possible to trigger DDI (Table 2). In addition, it was notable that the de-glycosylation of astragaloside IV (**B2**) to sapogenin-cycloastragenol strongly increased the inhibitory effects towards UGT1A8 (K_i = 0.034 μM) and 2B7 (K_i = 20.98 μM) [15]. Interestingly, naturally occurring ginsenosides, including ginsenosides Rg1 (**C6**), Rf (**C7**), Re (**C9**), Rd (**D2**), Rc (**D3**) and Rb1 (**D5**), were unlikely to cause clinically relevant DDI mediated *via* the induction or inhibition of most CYPs or UGTs involving in drug metabolism *in vivo*, which agreed with previous study [39].

Identification of the induction or inhibition of the abundant circulating alkaloids and saponins towards uptake and efflux transporters was another significant risk factor for the DDI. In clinics, oxymatrine (**A3**) could interfere with hOCT1-mediated hepatic uptake and renal elimination, and intestinal absorption by hOCT3, whereas matrine (**A1**) only had the potential to decrease hOCT3 expressed in enterocytes [40]. Besides, **A1** and **A3** did not demonstrate the inhibition of P-gp *in vitro* and *in vivo* [41]. Additionally, it was reported that astragaloside IV (**B2**) could induce the protein levels of P-gp, MRP1, MRP3, but produced the inhibitory effects on BCRP [42]. In contrast, in MDR1-MDCKII cells, **B2** only exhibited weak inhibition activity of 8.22% when treated with 100 μM [41]. Recently, several scholars got the fact that **B2** could induce the upregulation of P-gp and BCRP, and might be a potential substrate of P-gp [43]. For ginsenosides, ginsenoside Rg1 (**C6**) was potential inhibitor of NTCP (IC_{50} = 50.49 μM), whereas ginsenoside Re (**C9**) was potential substrates of NTCP [44]. Further, DDI between ginsenosides Rb1 (**D5**), Rc (**D3**), Rd (**D2**) and methotrexate (a probe substrate for Mrp2) might occur owing to the decrease in the mRNA and protein levels of Mrp2 [45]. In addition, **D5**, **D3**, **D2** and **D9** were predicted to possess the high potential for human OATP1B3-mediated drug interactions [16]. Moreover, PPT and PPD, the aglycones of *PPT-type* and *PPD-type* ginsenosides, respectively, were potent P-gp inhibitors, suggesting the unpredictable interactions when ginsenosides were co-administered with the P-gp substrate drugs [46]. The interactions of complex circulating compounds and clinical drugs based on transporters may be one of the important compatibility mechanisms for Kang-Ai injection.

In clinical consumption, the adverse drug reactions (ADR) derived from herbal injections, should be gaining more attention. It was essential to evaluate the objectivity of ADR, develop a reasonable application strategy, and ensure the security and validity of Kang-Ai injection. Data and information obtained from PK studies on the circulating alkaloids and saponins could help understand the complex action of herbal injections, and predict a variety of events related to the efficacy and toxicity of herbal injections. In Kang-Ai injection, the most abundant compounds, oxymatrine (**A3**) and matrine (**A1**) both could cause the hepatic toxicities, of which the toxicity of **A1** was greater than that of **A3** [47]. In addition, our results suggested that **A3** have inhibitory effects against CYP3A4 (IC_{50} = 8.81 μM) (Fig. 4B & Additional file 1: Table S8). These indicated that the elevated metabolism of **A3** by CYP3A4 would result in more severe liver damage, following the further influence on the protein expression and activity of CYP3A4 in the liver. It meant that many factors, especially ADR, should be monitored when **A3** was co-administered with clinical CYP3A4 substrate drugs. Therefore, the clarification of the PK studies could be helpful in deciphering the ADR and hepatorenal toxicity of herbal injections.

Conclusion

Herein, we identified 9 alkaloids, 6 astragalosides and 22 ginsenosides (Additional file 1: Table S1), which demonstrated relatively high levels of systemic exposure after dosing Kang-Ai injection, and assessed the PK behaviors and excretion (Table 1). Oxymatrine (**A3**) and matrine (**A1**) exhibited the most abundant systemic exposure of 68.61 and 502.71 μmol/L*h, respectively (Fig. 2A). And over 90% of dosed **A3** and **A1** were both mainly eliminated by the renal and hepatobiliary excretion. Furthermore, the saponins, i.e. astragaloside IV (**B2**), ginsenosides Rc (**D3**), Rd (**D2**), Rb1 (**D5**), Rg1 (**C6**), Re (**C9**), Rf (**C7**), Rb2 (**D4**) exhibited high exposure in plasma (> 500 nmol/L*h), whereas the $t_{1/2}$ values (4.12–7.22 hour) of *PPD-type* ginsenosides (**D2-D5**) were significantly longer than those (0.63–1.64 hour) of astragalosides (**B2**) and *PPT-type* ginsenosides (**C6**, **C7**, **C9**). Besides, unlike the elimination of **D2-D5** mainly attributing to renal excretion (Fig. 2B), the **B2** and **C6**, **C7**, **C9** were mainly excreted to urine and bile (Figs. 2B & 2C). The protein binding assays demonstrated that dosed **D2-D5** were extensively bound with $f_{u-plasma}$ values approximately 1%, while **B2** and *PPT-type* ginsenosides (**C6**, **C7**, **C9**) displayed the $f_{u-plasma}$ values of 12.35% and 60.23–87.36%, respectively (Table 1). Moreover, **A1** and **A3** exhibited weak inhibitory effects against CYP3A4 with IC_{50} values of 387.40 and 604.60 μM, respectively (Fig. 4 & Additional file 1: Table S8), while **B2**, **C6**, **C7**, **C9**, **D2**, **D3** and **D5** displayed weak or moderate inhibition towards several CYP and UGT enzymes with IC_{50} values ranging from 8.81 to 92.21 μM (Fig. 4 & Additional file 1: Table S8). The $[I]/K_i$ values were 1.15 for **A3** against CYP3A4 (Table 2), which seemed more possible to trigger DDI

risks. And other saponins displayed negligible DDI risk due to $[I]/K_i$ no more than 0.1 (Table 2). The current PK and excretion information gained here could serve as a crucial step in understanding the roles of circulating alkaloids, astragalosides and ginsenosides in therapeutic actions of Kang-Ai injection. These results here will also inform the potential DDI risks in clinical use of Kang-Ai injection.

Abbreviations

4-MU: 4-methylumbelliferone; AIC: Akaike information criterion; BCRP: breast cancer resistance protein; CYP: cytochrome P450; DDI: drug-drug interactions; hOCT: human organic cation transporter; HLM: human liver microsomes; IS: internal standard; LLOQ: lower limit of quantification; MDR1/P-gp: multidrug resistance protein 1; MRPs: multidrug resistance-associated proteins; MRM: multiple reactions monitoring; NADPH: nicotinamide adenine dinucleotide phosphate; OATP: organic anion transporting polypeptide; PK: pharmacokinetics (PK); QC: quality control; SC: Schwartz information criterion; UGT: UDP-glucuronosyltransferase; UDPGA: uridine 5'-diphosphoglucuronosyltransferase; UHPLC-TQD-MS: ultra high-performance liquid chromatography coupled with a triple quadrupole electrospray tandem mass spectrometry.

Declarations

Acknowledgements

The authors would like to thank Miss Panpan Yang for the UHPLC-TQD-MS tests.

Authors' contributions

Y-J and Y-Z conceived and designed the study; Q-ZF performed PK and enzyme inhibition assays; J-MM and X-H analyzed the data; Q-ZF, Y-J and Y-Z wrote this manuscript; Y-ZH, Z-XJ and Y-XS revised the manuscript. All authors read and approved the final manuscript

Funding

This work was supported by the National Natural Science Foundation of China (81903704, 81803638), Foundation of He'nan Educational Committee (20A350012), and National Major Scientific and Program of Introducing Talents of Discipline to Universities (B13038).

Availability of data and materials

Most of the data in the present study are included in this article and its additional information.

Ethics approval and consent to participate

The animal studies were in accordance with the Guide for the Care and Use of Laboratory Animals (National Institutes of Health). The study protocol was approved by the Ethics Review Committee for Animal Experimentation of Jinan University (Ethical Review NO. 20190301010).

Consent to publish

Not applicable.

Competing interests

The authors declare that they have no competing interests

References

1. Ning ZW, Zhai LX, Peng J, Zhao L, Huang T, Lin CY, Chen WH, Luo Z, Xiao HT, Bian ZX. Simultaneous UPLC-TQ-MS/MS determination of six active components in rat plasma: application in the pharmacokinetic study of Cyclocarya paliurus leaves. Chin Med. 2019;14:28.
2. Yao ZH, Qin ZF, He LL, Wang XL, Dai Y, Qin L, Gonzalez FJ, Ye WC, Yao XS. Identification, bioactivity evaluation and pharmacokinetics of multiple components in rat serum after oral administration of Xian-Ling-Gu-Bao capsule by ultra performance liquid chromatography coupled with quadrupole time-of-flight tandem mass spectrometry. J Chromatogr B. 2017;1041–1042:104 – 12.
3. Yan R, Yang Y, Chen Y. Pharmacokinetics of Chinese medicines: strategies and perspectives. Chin Med. 2018;13:24.
4. Lu T, Yang J, Gao X, Chen P, Du F, Sun Y, Wang F, Xu F, Shang H, Huang Y, Wang Y, Wan R, Liu C, Zhang B, Li C. Plasma and urinary tanshinol from Salvia miltiorrhiza (Danshen) can be used as pharmacokinetic markers for cardiotonic pills, a cardiovascular herbal medicine. Drug Metab Dispos. 2008;36(8):1578–86.
5. Cheng C, Du F, Yu K, Xu F, Wang F, Li L, Olaleye OE, Yang J, Chen F, Zhong C, Liu Q, Li J, Wang Z, Li C, Xiao W. Pharmacokinetics and Disposition of Circulating Iridoids and Organic Acids in Rats Intravenously Receiving ReDuNing Injection. Drug Metab Dispos. 2016;44(11):1853–8.
6. Lu Q, Li CL. Therapeutic efficacy and safety of Kang-ai injection combined with platinum-based doublet chemotherapy in advanced NSCLC: A meta-analysis. Life Sci. 2018;210:9–19.
7. He ZF, Wang JJ, Wang WD. Effect of Kangý ai Injection on Serum Level of Soluble Interleukin-2 Receptor and Vascular Endothelial Growth Factor in Patients with Esophageal Carcinoma during Radiotherapy. Chin J Integr Med. 2006;12(4):273–6.
8. Wan YM, Li YH, Xu ZY, Wu HM, Xu Y, Yang M, Wu XN. The Effect of Transarterial Chemoembolization in Combination With Kang'ai Injection on Patients With Intermediate Stage Hepatocellular Carcinoma: A Prospective Study. Integr Cancer Ther. 2018;17(2):477–85.
9. Jia M, Zhang B, Qi Y, Yang J, Yao Z, Qin Z, Zhang X, Yao X. Ultra high-performance liquid chromatography coupled with mass spectrometry and chemometric analysis of Kang-Ai injection based on the chemical characterization, simultaneous quantification and relative quantification of forty-seven herbal alkaloids and saponins. J Sep Sci. 2020. DOI:10.1002/jssc.201900878.
10. Yang J, Dai G, Hou Y, Song Z, Wang F, Ji G, Chen J. Quantification of oxymatrine in rat plasma by UPLC-MS/MS to support the pharmacokinetic analyses of oxymatrine-loaded polymersomes. Anal Methods. 2014;6(6):1811–7.
11. Wu XL, Hang TJ, Shen JP, Zhang YD. Determination and pharmacokinetic study of oxymatrine and its metabolite matrine in human plasma by liquid chromatography tandem mass spectrometry. J Pharm Biomed Anal. 2006;41(3):918–24.

12. Xu M, Yin J, Xie L, Zhang J, Zou C, Zou J, Liu F, Ju W, Li P. Pharmacokinetics and tolerance of toal astragalosides after intravenous infusion of astragalosides injection in healthy Chinese volunteers. Phytomedicine. 2013;20(12):1105–11.
13. Jin Y, Guo X, Yuan B, Yu W, Suo H, Li Z, Xu H. Disposition of Astragaloside IV via Enterohepatic Circulation Is Affected by the Activity of the Intestinal Microbiome. J Agric Food Chem. 2015;63(26):6084–93.
14. Zhang WD, Zhang C, Liu RH, Li HL, Zhang JT, Mao C, Moran S, Chen CL. Preclinical pharmacokinetics and tissue distribution of a natural cardioprotective agent astragaloside IV in rats and dogs. Life Sci. 2006;79(8):808–15.
15. Ran R, Zhang C, Li R, Chen B, Zhang W, Zhao Z, Fu Z, Du Z, Du X, Yang X, Fang Z. Evaluation and Comparison of the Inhibition Effect of Astragaloside IV and Aglycone Cycloastragenol on Various UDP-Glucuronosyltransferase (UGT) Isoforms. Molecules. 2016;21:1616.
16. Olaleye OE, Niu W, Du FF, Wang FQ, Xu F, Pintusophon S, Lu JL, Yang JL, Li C. Multiple circulating saponins from intravenous ShenMai inhibit OATP1Bs in vitro: potential joint precipitants of drug interactions. Acta Pharmacol Sin. 2018;40(6):833–49.
17. Yao Z, Li S, Qin Z, Hong X, Dai Y, Wu B, Ye W, Gonzalez FJ, Yao X. Characterization of human UDP-glucuronosyltransferases responsible for glucuronidation and inhibition of norbakuchinic acid, a primary metabolite of hepatotoxicity and nephrotoxicity component bakuchiol in Psoralea corylifolia L. RSC Adv. 2017;7:52661–71.
18. Gao L, Qin Z, Zhang B, Yin Z, Yang XZJ. An investigation of the metabolic activity, isozyme contribution, species differences and potential drug–drug interactions of PI-103, and the identification of efflux transporters for PI-103-Oglucuronide in HeLa1A9 cells. RSC Adv. 2020;10:9610–22.
19. Sun ZH, Chen J, Song YQ, Dou TY, Zou LW, Hao DC, Liu HB, Ge GB, Yang L. Inhibition of human carboxylesterases by ginsenosides: structure-activity relationships and inhibitory mechanism. Chin Med. 2019;14:56.
20. Ge G. Deciphering the metabolic fates of herbal constituents and the interactions of herbs with human metabolic system. Chin J Nat Med. 2019;17(11):801–2.
21. Lv X, Xia Y, Finel M, Wu J, Ge G, Yang L. Recent progress and challenges in screening and characterization of UGT1A1 inhibitors. Acta Pharm Sin B. 2019;9(2):258–78.
22. Zhou QH, Zhu YD, Zhang F, Song YQ, Jia SN, Zhu L, Fang SQ, Ge GB. Interactions of drug-metabolizing enzymes with the Chinese herb Psoraleae Fructus. Chin J Nat Med. 2019;17(11):858–70.
23. US Food and Drug Administration. Guidance for Industry, Bioanalytical Method Validation, 2013 http://www.fda.gov/downloads/drugs/.
24. Matuszewski BK, Constanzer ML, Chavez-Eng CM. Matrix effect in quantitative LC/MS/MS analyses of biological fluids: a method for determination of finasteride in human plasma at picogram per milliliter concentrations. Anal Chem. 1998;70(5):882–9.
25. Reagan-Shaw S, Nihal M, Ahmad N. Dose translation from animal to human studies revisited. FASEB J. 2008;22(3):659–61.
26. Guo B, Li C, Wang G, Chen L. Rapid and direct measurement of free concentrations of highly protein-bound fluoxetine and its metabolite norfluoxetine in plasma. Rapid Commun Mass Spectrom. 2006;20(1):39–47.
27. He W, Wu JJ, Ning J, Hou J, Xin H, He YQ, Ge GB, Xu W. Inhibition of human cytochrome P450 enzymes by licochalcone A, a naturally occurring constituent of licorice. Toxicol In Vitro. 2015;29(7):1569–76.
28. Xin H, Qi XY, Wu JJ, Wang XX, Li Y, Hong JY, He W, Xu W, Ge GB, Yang L. Assessment of the inhibition potential of Licochalcone A against human UDP-glucuronosyltransferases. Food Chem Toxicol. 2016;90:112–22.
29. Huang LH, Zhong YM, Xiong XH, Cen MF, Cheng XG, Wang GX, Chen JS, Wang SJ. The Disposition of Oxymatrine in the Vascularly Perfused Rat Intestine-Liver Preparation and Its Metabolism in Rat Liver Microsomes. J Pharm Sci. 2016;105(2):897–903.

30. Lin P, Dai Y, Yao Z, Qin Z, He L, Wang Q, Wei Z, Zhang Y, Yao X. Metabolic profiles and pharmacokinetics of Qingre Xiaoyanning capsule, a traditional Chinese medicine prescription of Sarcandrae Herba, in rats by UHPLC coupled with quadrupole time-of-flight tandem mass spectrometry. J Sep Sci. 2019;42(4):784–96.
31. Liu XW, Yang JL, Niu W, Jia WW, Olaleye OE, Wen Q, Duan XN, Huang YH, Wang FQ, Du FF, Zhong CC, Li YF, Xu F, Gao Q, Li L, Li C. Human pharmacokinetics of ginkgo terpene lactones and impact of carboxylation in blood on their platelet-activating factor antagonistic activity. Acta Pharmacol Sin. 2018;39(12):1935–46.
32. Davies B, Morris T. Physiological parameters in laboratory animals and humans. Pharm Res. 1993;10(7):1093–5.
33. Halim CE, Xinjing SL, Fan L, Bailey Vitarbo J, Arfuso F, Tan CH, Narula AS, Kumar AP, Sethi G, Ahn KS. Anti-cancer effects of oxymatrine are mediated through multiple molecular mechanism(s) in tumor models. Pharmacol Res. 2019;147:104327.
34. Rashid HU, Xu Y, Muhammad Y, Wang L, Jiang J. Research advances on anticancer activities of matrine and its derivatives: An updated overview. Eur J Med Chem. 2019;161:205–38.
35. Li L, Hou X, Xu R, Liu C, Tu M. Research review on the pharmacological effects of astragaloside IV. Fundam Clin Pharmacol. 2017;31(1):17–36.
36. Mancuso C, Santangelo R. Panax ginseng and Panax quinquefolius: From pharmacology to toxicology. Food Chem Toxicol. 2017;107:362–72.
37. Liu W, Shi J, Zhu l, Luo D, Zhao F, Wang M, Hu Y, Lu M, Liu l. Z. Reductive metabolism of oxymatrine is catalyzed by microsomal CYP3A4. Drug Des Devel Ther. 2015;9:5771–83.
38. Yang Z, Gao S, Yin T, Kulkarni KH, Teng Y, You M, Hu M. Biopharmaceutical and pharmacokinetic characterization of matrine as determined by a sensitive and robust UPLC–MS/MS method. J Pharm Biomed Anal. 2010;51(5):1120–7.
39. Seong SJ, Kang WY, Heo JK, Jo J, Choi WG, Liu KH, Lee S, Choi MK, Han YH, Lee HS, Ohk B, Lee HW, Song IS, Yoon YR. A Comprehensive In Vivo and In Vitro Assessment of the Drug Interaction Potential of Red Ginseng. Clin Ther. 2018;40(8):1322–37.
40. Pan X, Wang L, Gründemann D, Sweet DH. Inhibition of human organic cation transporters by the alkaloids matrine and oxymatrine. Fitoterapia. 2014;92:206–10.
41. Li X, Hu J, Wang B, Sheng L, Liu Z, Yang S, Li Y. Inhibitory effects of herbal constituents on P-glycoprotein in vitro and in vivo: Herb–drug interactions mediated via P-gp. Toxicol Appl Pharmacol. 2014;275(2):163–75.
42. Zhang G, Ou R, Li F, Wu J, Zheng L, Tong Y, Liu Y, Liu Z, Lu L. Regulation of drug-metabolizing enzymes and efflux transporters by Astragali radix decoction and its main bioactive compounds: Implication for clinical drug-drug interactions. J Ethnopharmacol. 2016;180:104–13.
43. Zhang W, Liu M, Yang L, Huang F, Lan Y, Li H, Wu H, Zhang B, Shi H, Wu X. P-glycoprotein Inhibitor Tariquidar Potentiates Efficacy of Astragaloside IV in Experimental Autoimmune Encephalomyelitis Mice. Molecules. 2019;24:561.
44. Zhan T, Yao N, Wu L, Lu Y, Liu M, Liu F, Xiong Y, Xia C. The major effective components in Shengmai Formula interact with sodium taurocholate co-transporting polypeptide. Phytomedicine. 2019;59:152916.
45. Lee S, Kwon M, Choi MK, Song IS. Effects of Red Ginseng Extract on the Pharmacokinetics and Elimination of Methotrexate via Mrp2 Regulation. Molecules. 2018;23:2948.
46. Li N, Wang D, Ge G, Wang X, Liu Y, Yang L. Ginsenoside metabolites inhibit P-glycoprotein in vitro and in situ using three absorption models. Planta Med. 2014;80(4):290–6.
47. Zhang Q, Li FJ, Jin RM, Song ZP. Study on the hepatotoxicity induced by matrine and oxymatrine. Chinese Archives of Traditional Chinese Medicine. 2011;29:1222–5.

Supplementary Information

Additional file 1: Table S1. Information of unchanged compounds in rats after a 30 min-infusion of Kang-Ai injection (6 mL/kg) by UHPLC/Q-TOF-MS. **Table S2**. Linear correlation parameters, limits of detection (LODs) and lower limits of quantification (LLOQs) of each circulating compound in rat plasma after a 30 min-infusion of Kang-Ai injection (6 mL/kg). **Table S3**. Relative standard deviation (RSD) values of intra-day and inter-day precisions, and of sixteen compounds in rat plasma after a 30 min-infusion of Kang-Ai injection (6 mL/kg). **Table S4**. Matrix effect and extraction recovery of each compound and two internal standard (IS) in rat plasma after a 30 min-infusion of Kang-Ai injection (6 mL/kg). **Table S5**. Stability results of each compound and internal standard in rat plasma after a 30 min-infusion of Kang-Ai injection (6 mL/kg). **Table S6**. Linear correlation parameters, LLOQs of twenty analytes in rat urine after a 30 min-infusion of Kang-Ai injection (6 mL/kg). **Table S7**. Linear correlation parameters, LLOQs of twenty-one analytes in rat bile after a 30 min-infusion of Kang-Ai injection (6 mL/kg). **Table S8**. The IC_{50} values of six circulating alkaloids and saponins towards several recombinant CYP and UGT isozymes. Data represent the mean ± standard deviation of triplicate. **Fig S1**. Chemical structures (A) and content levels (B) of circulating alkaloids, astragalosides and ginsenosides in rats after intravenous Kang-Ai injection (6 mL/kg). See Supporting Information Table S1 for compounds identification and names. **Fig S2**. Representative MRM chromatograms of sixteen circulating compounds in plasma. (A) blank plasma, (B) blank plasma spiked with sixteen analytes at LLOQ, (C) rat plasma samples at 0.5 h after an intravenous 30 min-infusion of Kang-Ai injection.

Figures

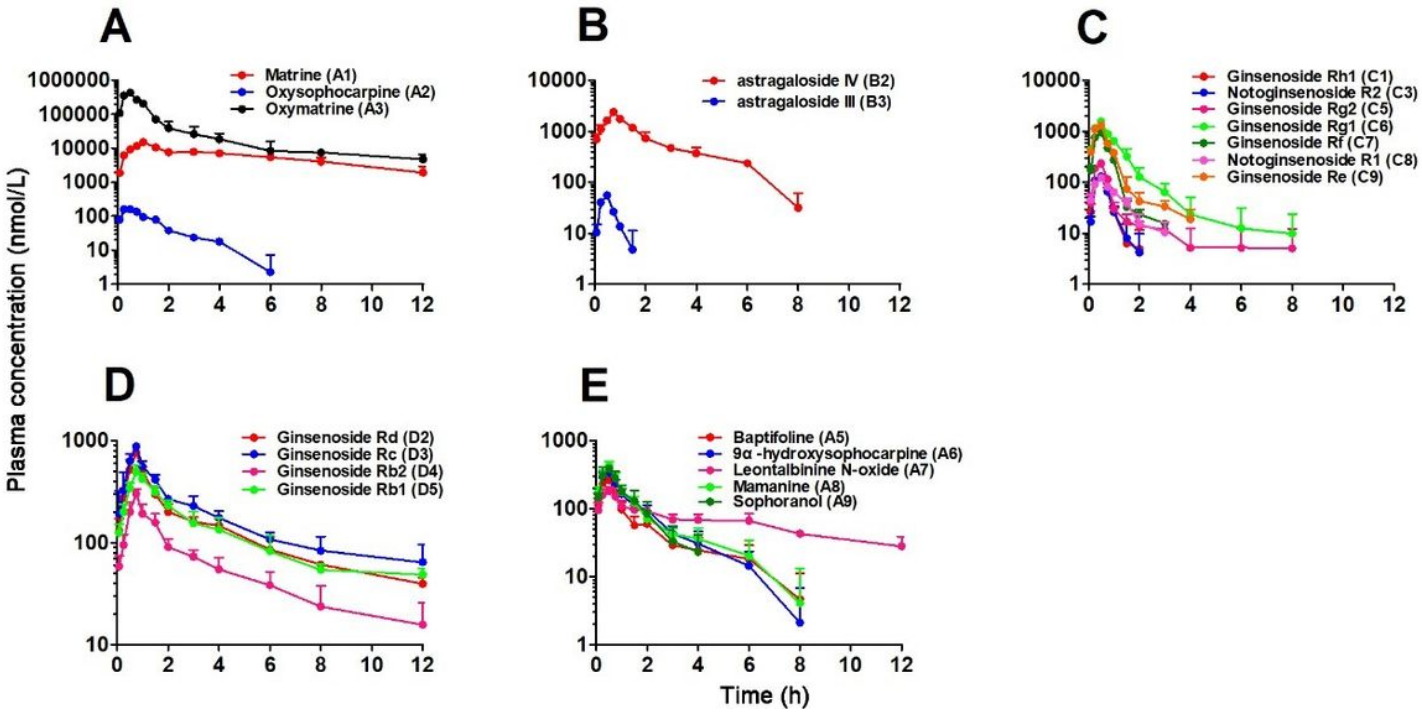

Figure 1

Mean plasma pharmacokinetics of three abundant alkaloids (A), two astragalosides (B), seven PPT-type ginsenosides (C), four PPD-type ginsenosides (D) and other five minor alkaloids (E) over the time after receiving an intravenous 30-min infusion of Kang-Ai injection in rats (6 mL/kg). See Supporting Information Table S1 for the compounds' ID and names.

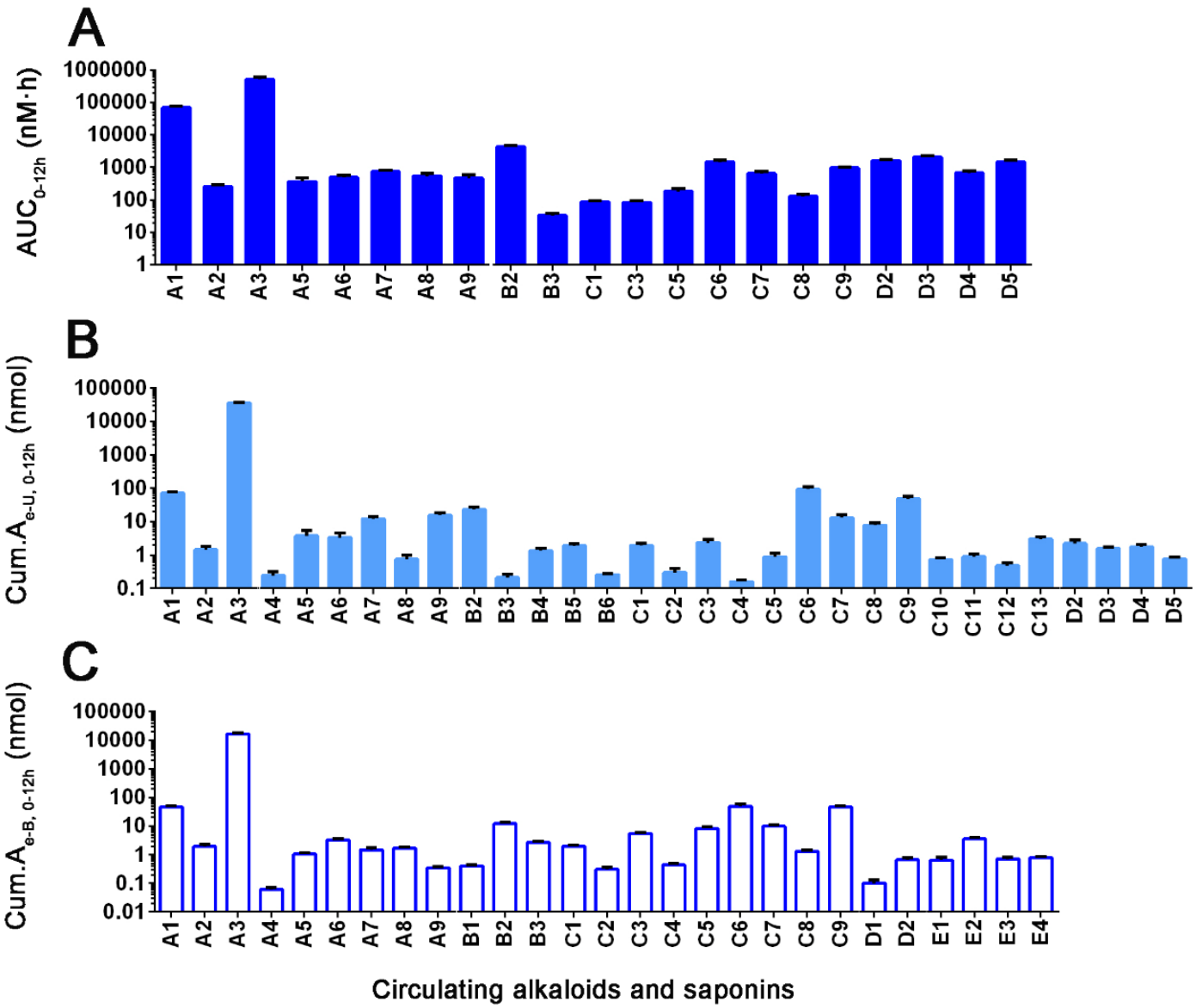

Figure 2

Systemic exposure in plasma (A), renal excretion in urine (B) and hepatobiliary excretion in bile (C) of circulating alkaloids, astragalosides and ginsenosides after a 30-min intravenous infusion of Kang-Ai injection to rats (6 mL/kg). See Supporting Information Table S1 for the compounds' ID and names.

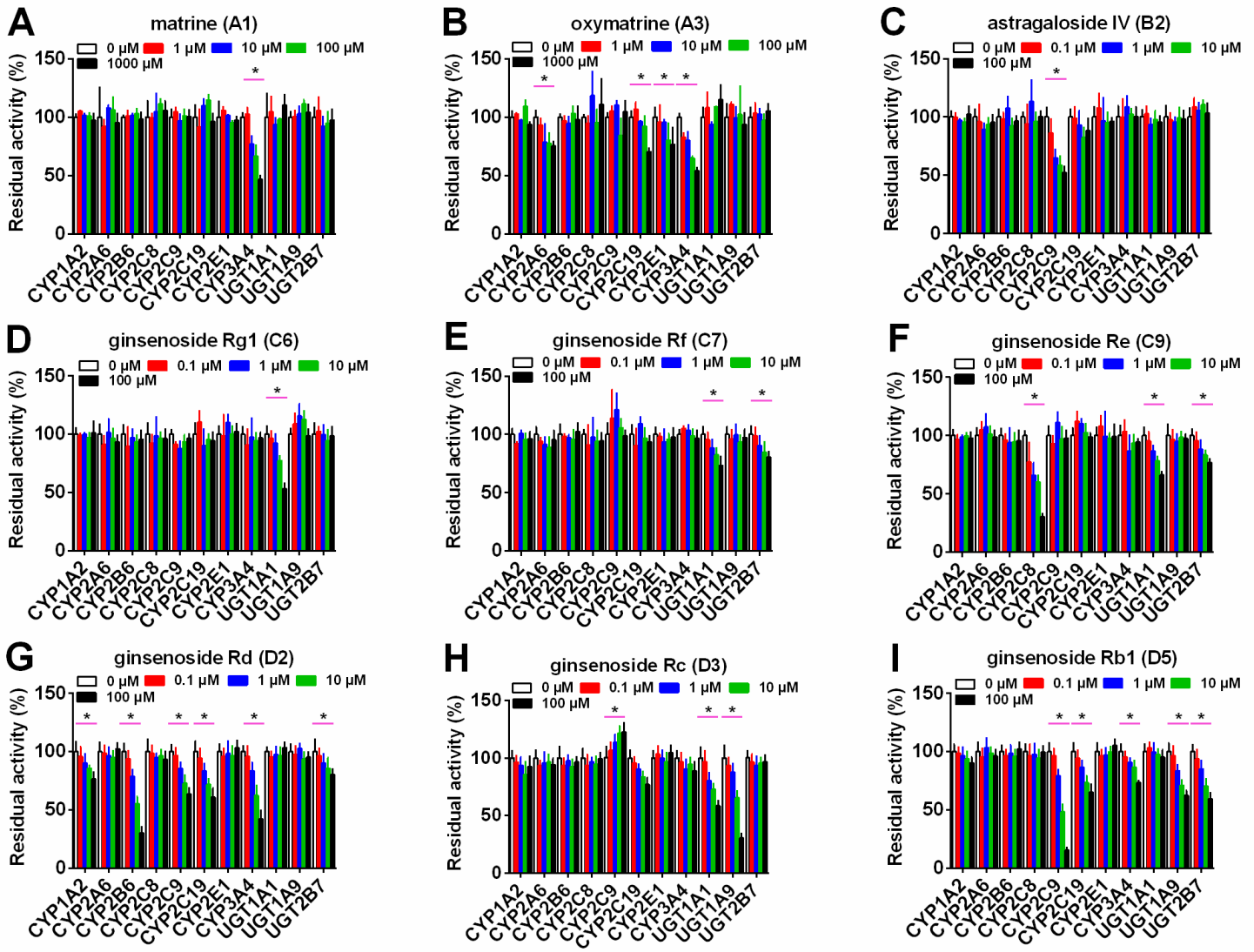

Figure 3

The effects of several circulation compounds towards eight expressed CYP isozymes and three recombinant UGT enzymes. (A) matrine, (B) oxymatrine, (C) astragaloside IV, (D) ginsenoside Rg1, (E) ginsenoside Rf, (F) ginsenoside Re, (G) ginsenoside Rd, (H) ginsenoside Rc, (I) ginsenoside Rb1; The probe substrates were incubated at 37 ºC in the absence (control, 0 μM) and presence of tested compounds (1, 10, 100 and 1000 μM for matrine and oxymatrine; 0.1, 1, 10 and 100 μM for astragaloside and ginsenoside). Data represent the mean ± standard deviation of triplicate, (* compared with those of control, * $p < 0.05$).

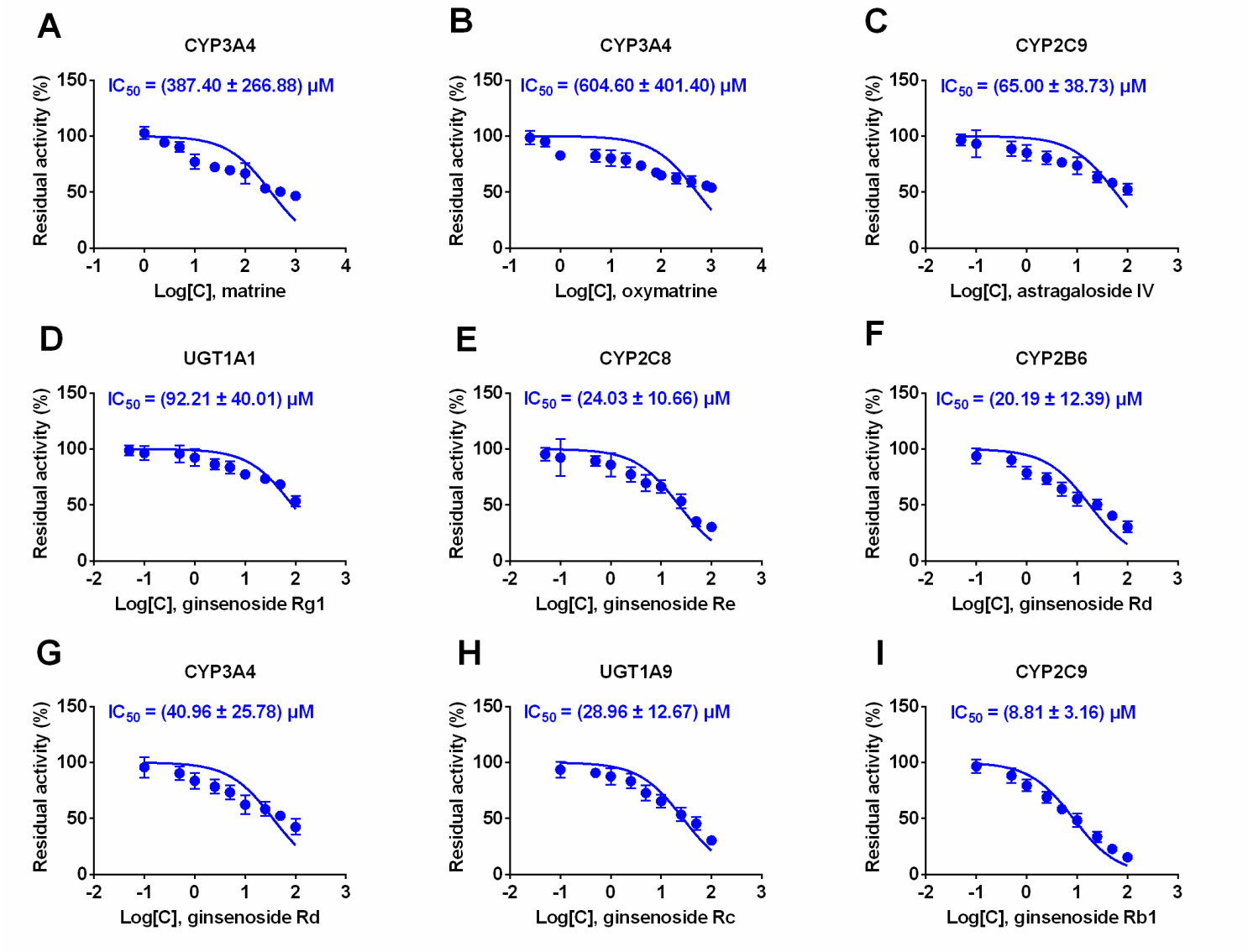

Figure 4

The IC50 values of matrine against CYP3A4 (A), oxymatrine towards CYP3A4 (B), astragaloside IV against CYP2C9 (C), ginsenoside Rg1 against UGT1A1 (D), ginsenoside Re towards CYP2C8 (E), ginsenoside Rd towards CYP2B6 (F) and CYP3A4 (G), ginsenoside Rc against UGT1A9 (H), and ginsenoside Rb1 against CYP2C9 (I). The data were fit to log (I) and normalized response equations. Each data point represented the mean value ± the S.D. of triplicate determination.

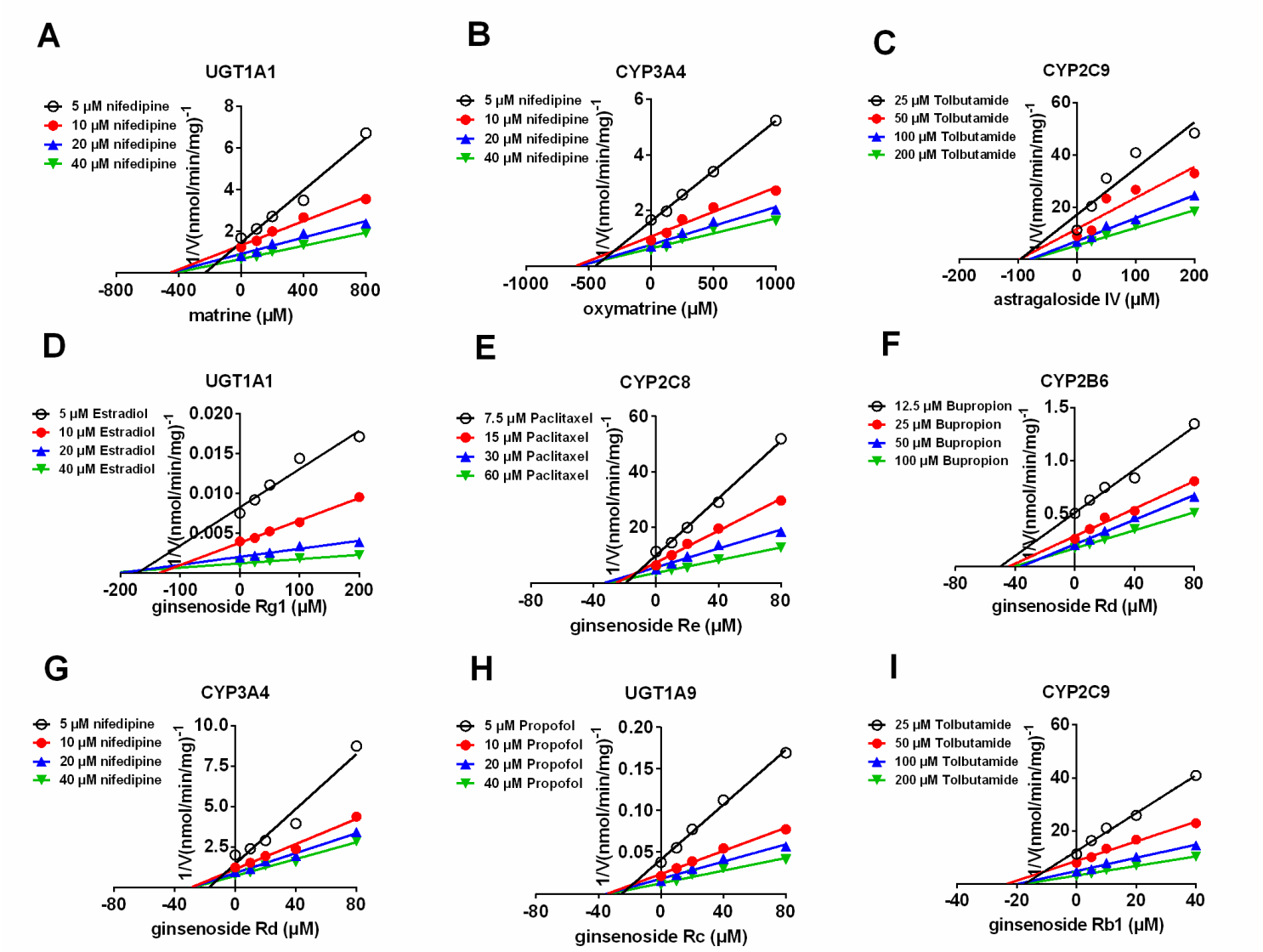

Figure 5

The Dixon plots for the inhibition effects of circulating alkaloids and saponins against recombinant CYP and UGT isozymes. (A) Inhibition effect of matrine against nifedipine-oxidation for CYP3A4; (B) Inhibition effect of oxymatrine towards nifedipine-oxidation for CYP3A4; (C) Inhibition effect of astragaloside IV against tolbutamide-4-hydroxylation for CYP2C9; (D) Inhibition effect of ginsenoside Rg1 towards β-estradiol-3-O-glucuronidation for UGT1A1; (E) Inhibition effect of ginsenoside Re against paclitaxel-6-hydroxylation for CYP2C8; (F) Inhibition effect of ginsenoside Rd towards bupropion-hydroxylation for CYP2B6; (G) Inhibition effect of ginsenoside Rd against nifedipine-oxidation for CYP3A4; (H) Inhibition effect of ginsenoside Rc towards propofol-O-glucuronidation for UGT1A9; (I) Inhibition effect of ginsenoside Rb1 against tolbutamide-4-hydroxylation for CYP2C9; All data represent the means ± SD of triplicate determinations.

Supplementary Files

This is a list of supplementary files associated with this preprint. Click to download.

- Supplementaryinformation.docx